Modal analysis of historical masonry structures: linear perturbation and software benchmarking

Daniele Pellegrini[a], Maria Girardi[a], Paulo B. Lourenço[b], Maria Giovanna Masciotta[b], Nuno Mendes[b], Cristina Padovani[a], Luis F. Ramos[b]

[a] *Institute of Information Science and Technologies "A. Faedo", ISTI–CNR, Pisa, Italy*
[b] *ISISE, University of Minho, Department of Civil Engineering, Guimarães, Portugal*

Abstract

The mechanical behavior of masonry materials has a common feature: a nonlinear behavior with high compressive strength and very low tensile strength. As a consequence, old masonry buildings generally present cracks due to permanent loads and/or accidental events. Therefore, the characterization of the global dynamic behavior of masonry structures should take into account the presence of existing cracks. This paper presents a numerical approach coupling linear perturbation and modal analysis in order to estimate the dynamic properties of masonry constructions, taking into account the existence of structural damage. First, the approach is validated on a masonry arch subjected to increasing loads, via three FE codes. Then, the same procedure is applied to a real masonry structure affected by a severe crack distribution.

Keywords: Masonry-like materials, masonry constructions, modal analysis, numerical methods, nonlinear elasticity, linear perturbation

1. Introduction

Safeguarding of cultural heritage is an acquired principle nowadays, widely shared by all communities. Preservation of the past is an indispensable requirement for our society to foster knowledge, awareness of identity, and ability to think of and plan the future. With regard to architectural heritage, age-old buildings and monuments need to be preserved not only from damage mechanisms and deterioration processes induced by anthropogenic and environmental actions, but also from the aging effects they are exposed to during their lifetime. Furthermore, ancient structures are particularly vulnerable to seismic actions, whose consequences should be prevented - or at least mitigated - with effective strengthening measures and maintenance plans. For this purpose, Structural Health Monitoring (SHM) and Finite Element (FE) analysis represent complementary techniques which may help to understand the complex dynamic behavior of ancient buildings and estimate the mechanical properties of their constituent materials with use of limited invasive testing procedures. In addition, if long–term monitoring protocols are conducted, important information can be catched on the interactions between the structure under consideration and the surrounding environment [4], [44], as well as on the evolution of the structural health over time. In fact, significant changes in the structure's dynamic properties can reveal the presence of structural damage, as pointed out in [21], [40], [43], where decreasing values of natural frequencies were measured at the onset of damage. Moreover, dynamic monitorig can represent a valuable tool to assess the effectiveness of strengthening interventions, as shown in [33], [34], [44], where evident rising in the natural frequencies was observed in the monitored historical structures after restoration works.

Structural health monitoring is usually coupled with FE analysis via model updating procedures [1], [2], [5], **[10]**, [12], [46], [52], in order to derive realistic information about the boundary conditions and the mechanical properties of the structure's constituent materials, especially when more invasive techniques are not viable as in case of heritage buildings. These procedures typically consist in tuning some parameters of the FE model in order to minimize the distance between numerical and experimental modal properties (natural frequencies and mode shapes).

In this regard, it is worth noting that modal analysis is carried out within the framework of linear elasticity. This setting could be unsuited for masonry buildings, which may exhibit nonlinear behavior even for the self–weight and sometimes show extended crack patterns. Therefore, the dynamic behavior of these constructions should be analyzed by taking into account the existing damage so as to avoid erroneous evaluations of the parameters, which may in turn compromise the outcome of further numerical simulations. A common approach to this problem consists in simulating the actual damage observed on the structure by reducing the stiffness of those finite elements belonging to the cracked or damaged parts [7], **[10]**, [41], [43].

In [23] a numerical procedure implemented in the non commercial FE software NOSA–ITACA (www.nosaitaca.it) is described. Here, the masonry material is modeled via the masonry–like constitutive equation [14], [30]. This procedure allows evaluating the natural frequencies and mode shapes of masonry buildings in the presence of cracks, via linear perturbation analysis and consists of the following steps: first, the initial loads and boundary conditions are applied to the FE model and the resulting nonlinear equilibrium problem is solved through an iterative scheme. Then, a modal analysis about the equilibrium solution is performed, by using the tangent stiffness matrix calculated in the last iteration before convergence is reached, thereby allowing the user to automatically take into account the effects of the stress distribution on the structure's stiffness.

Other applications of linear perturbation, sometimes referred to as prestressed modal analysis, are in the framework of large deformation problems [13], [24], [36], [53]. With regard to masonry buildings, an example is shown in [18], where linear perturbation is applied via a commercial code to a historic masonry building.

This paper focuses on the use of linear perturbation to evaluate modal properties of ancient masonry buildings in the presence of cracks. The method is described in Section 2 and applied to a masonry arch in Section 3, where the results obtained via different constitutive equations and FE codes (DIANA, MARC, NOSA-ITACA) are compared and discussed. Then, a real case application is presented in Section 4, where the Mogadouro clock tower is analyzed via the NOSA-ITACA code, before and after the restoration works carried out in 2005. The paper demonstrates that, by adopting the appropriate constitutive model, different FE codes do provide the same modal features in the presence of a damaged structure. Moreover, making use of the experimental results at the authors' disposal [44], [45], it is shown that linear perturbation analysis combined with finite element modal updating allows identifying the tower's material properties (i.e. Young's modulus and tensile strength) that consistently reflect the damaged condition of the structure before restoration as well as the increase of the structural stiffness resulting from the subsequent strengthening intervention.

2. Constitutive equations, linear perturbation and modal analysis

In recent years the advancement of computer technology and introduction of innovative mathematical models made it possible to assess the structural safety of complex ancient masonry buildings by taking into account the nonlinear behavior of masonry materials, whose response to tension is completely different from that to compression and whose mechanical characteristics are the result of both their constituent elements and the building techniques used. The numerous studies conducted in the last decades, aimed at modeling the behavior of masonry structures, led to the formulation of different constitutive laws that can be grouped into two main classes. The first class includes those models in which the macroscopic behavior of the masonry material is obtained from the micro-mechanical behavior of its singular components [37], [50], [48], [26], [16], [17]. The second class contains instead the so-called macro-mechanical models, in which the masonry material is modeled either as an equivalent continuum [6], [14], [30], [51], [35], or as an assembly of macro elements with few degrees of freedom characterized by certain global behaviors [25], [39], [49]. Models originally formulated for concrete and subsequently applied to masonry structures [9], [47], [11] can be included in this latter group. A comprehensive review of constitutive models for masonry falls outside the scope of this paper and the reader is referred to [27], [28], [29] and [42] for a thorough discussion.

When dealing with the analysis of ancient masonry buildings, constitutive equations belonging to the second class are preferable. In fact, the application of micro-mechanical models is not straightforward, since it is difficult to identify a homogeneous and/or periodic structure in historical masonries. Moreover, the use of micro-mechanical models requires accurate knowledge of several parameters related to mechanical properties of the masonry constituent elements, which can not be easily determined; furthermore, the employment of the micro-mechanical models to complex structures calls for high computational cost. On the other hand, the application of macro-mechanical models does require the knowledge of a few parameters, which can be obtained from experimental tests, literature values or even from indications provided by national building codes and regulations.

Among macro–mechanical models, the constitutive equation for low tension materials, implemented in MARC [32], and the Rankine model, implemented in DIANA [15], are largely adopted to simulate the structural behavior of masonry constructions. Along with these models, both based on the theory of infinitesimal plasticity, the nonlinear elastic equation of masonry-like materials [30] is able to realistically describe the behavior of masonry buildings by taking into consideration their zero or low tensile strength. This constitutive equation has been implemented in NOSA-ITACA [8], [22], a finite element code developed and freely distributed by ISTI-CNR (www.nosaitaca.it). Here, masonry is modeled as an isotropic nonlinear elastic material with zero tensile strength and infinite compressive strength [14]. It is possible to prove that for every infinitesimal strain tensor $\mathbf{E}$, there exists a unique triplet $(\mathbf{T}, \mathbf{E}^e, \mathbf{E}^f)$ of symmetric tensors such that $\mathbf{E}$ is the sum of an elastic strain $\mathbf{E}^e$ and a positive semidefinite fracture strain $\mathbf{E}^f$, and the Cauchy stress $\mathbf{T}$, negative semidefinite and orthogonal to $\mathbf{E}^f$, depends linearly and isotropically on $\mathbf{E}^e$, through the Young's modulus E and Poisson's ratio ν [14], [30].

Masonry-like materials are then characterized by the stress function $\mathbb{T}$ given by $\mathbb{T}(\mathbf{E}) = \mathbf{T}$, whose explicit expression is reported in [30], along with its properties. In particular, $\mathbb{T}$ is differentiable in an open dense subset of the set of all strains [38] and the derivative $D_E\mathbb{T}(\mathbf{E})$ of $\mathbb{T}(\mathbf{E})$ with respect to $\mathbf{E}$ is a positive semidefinite symmetric fourth–order tensor, whose explicit expression is reported in [30]. The equation of masonry-like materials has been then generalized in order to take into account a weak tensile strength $\sigma_t \geq 0$ [30].

The constitutive law of low tensile materials implemented in MARC [32] is based on the nonlinear concrete cracking formulation described in [9]. Masonry is modeled as a nonlinear isotropic material in which a crack can develop orthogonal to the direction of the maximum principal stress, when it exceeds the strength of the material σ_t. After the occurrence of the first crack, a second crack may arise orthogonal to the first. In the same way, a third crack could open perpendicularly to the first two. In this situation the material loses all its load-carrying capacity across the crack, except when a tension softening behavior is considered, which can have a linear trend with slope equal to E_s.

The Rankine plasticity model implemented in DIANA [15] employes the Rankine yield criterion to simulate tensile cracking in concrete and rock under monotonic loading conditions. The yield function depends on both the maximum principal stress and a yield value $\tilde{\sigma}_t$ that describes the nonlinear exponential tensile softening behavior of the material, involving the tensile strength σ_t and the fracture energy $G_{\mathrm{f}}^{\mathrm{I}}$ [19].

Although the mechanical behavior of masonry constructions is clearly nonlinear, modal analysis, which is based on the assumption that masonry constituent materials feature a linear elastic behavior, is widely used in practical applications. Indeed, it provides important qualitative information on the global dynamic behavior of masonry structures, thereby allowing to assess their seismic vulnerability in compliance with the Italian and European regulations. On the other hand, traditional modal analysis does not take into account the influence that both the nonlinear behavior of the masonry material and the presence of cracked regions can have on the natural frequencies of masonry structures. While the effects of cracks on the vibration frequencies are taken into account in different fields of mechanical and aerospace engineering through the so-called linear perturbation analysis, such effects are not fully explored yet as far as the civil engineering field is concerned.

In this paper the linear perturbation approach is coupled with modal analysis, with the aim of assessing the dependence of the dynamic properties of a masonry structure on the stress field and crack distribution induced by the loads acting on the structure. Apart from the examples described in [23], where a masonry beam, an arch on piers and the San Frediano bell tower in Lucca have been analyzed, coupling linear perturbation and modal analysis is far from being fully investigated, although it allows for calculating the natural frequencies and mode shapes of a masonry body exhibiting a crack distribution due to the applied loads. In this regard, the procedure implemented in the NOSA–ITACA code consists in calculating the numerical solution to the nonlinear equilibrium problem of a masonry structure discretized into finite elements, subjected to given boundary and loading conditions, and then considering the linear equation governing the undamped free vibrations of the structure about the equilibrium state

$$M\ddot{u} + K_{\mathrm{T}}u = 0. \tag{1}$$

In equation (1) u is the displacement vector, which belongs to $\mathbb{R}^n$ and depends on time t, $\ddot{u}$ is the second-derivative of u with respect to t, and

K_{T} and $M \in \mathbb{R}^{n\times n}$ are the tangent stiffness and mass matrices of the finite-element assemblage. Note that K_{T} is symmetric and positive semidefinite, M is symmetric and positive definite. Equation (1) is similar to the equation of the motion of a linear elastic body, though here the elastic stiffness matrix, calculated using the elasticity tensor, is replaced by the tangent stiffness matrix K_{T}, calculated using the solution to the equilibrium problem and then takes into account the presence of cracks in body.

By assuming that

$$u = \phi \sin(\omega t), \tag{2}$$

with ϕ a vector of $\mathbb{R}^n$ and ω a real scalar, equation (1) can be transformed into the constrained generalized eigenvalue problem

$$K_{\mathrm{T}}\, \phi = \omega^2\, M\, \phi, \tag{3}$$

$$T\phi = 0, \tag{4}$$

with $T \in \mathbb{R}^{m\times n}$ and $m \ll n$.

Condition (4) expresses the fixed constraints and the master-slave relations assigned to displacement u, written in terms of vector ϕ. The restriction of the matrix K_{T} to the null subspace of $\mathbb{R}^n$ defined by (4) is positive definite.

Therefore, given the structure under examination, discretized into finite elements, and given the mechanical properties of the constituent materials together with the kinematic constraints and loads acting on the structure, the procedure implemented in NOSA-ITACA consists of the following steps.

Step 1. A preliminary modal analysis is conducted by assuming the structure's constituent material to be linear elastic, with stiffness matrix K. The generalized eigenvalue problem (3)-(4) is then solved, with K in place of K_{T}, and the natural frequencies $f_{\mathrm{i,E}} = \omega_{\mathrm{i,E}}/2\pi$ and mode shapes ϕ_{i}^{l} calculated.

Step 2. The solution of the nonlinear equilibrium problem of the structure is found and the derivative of the stress function needed to calculate the tangent stiffness matrix K_{T} to be used in the next step is evaluated.

Step 3. The generalized eigenvalue problem (3)-(4) is finally solved and the natural frequencies $f_{\mathrm{i}} = \omega_{\mathrm{i}}/2\pi$ of the structure in the presence of cracks are estimated.

Similar procedures based on linear perturbation followed by modal analysis are implemented in MARC and DIANA. The three codes NOSA-ITACA, MARC and DIANA, which adopt different constitutive equations for masonry, have been used with the twofold aim of (1) studying the static behavior of a masonry arch subjected to its own weight and a vertical concentrated load and, after a linear perturbation, (2) assessing the dependence of the natural frequencies and mode shapes on the crack distribution. The results of this comparative study are reported in Section 3 and show that, in spite of the different constitutive equations adopted, the dependence of the dynamical properties of the arch on the loads is very similar for the three codes.

3. Application to a masonry arch and software benchmarking

The numerical method for modal analysis described in Section 2 is here applied to the semi-circular masonry arch shown in Figure 1. The system is fully clamped at the springings and its geometry features a mean radius of 0.77 m, a span of 1.50 m, a cross section of 0.16 m$\times$1 m and a springing angle of about 13°. The arch is subjected to a plane stress state due to its self-weight and to a concentrated load P applied at the extrados at a quarter of the span. The arch is discretized into 784 8-node isoparametric quadrilateral elements with quadratic shape functions (corresponding to element 2, 26 and CQ16M of the NOSA-ITACA [8], MARC [32] and DIANA [15] libraries, respectively), for a total of 2565 nodes. Figure 2 shows the mesh generated by NOSA-ITACA, later converted in the MARC and DIANA format.

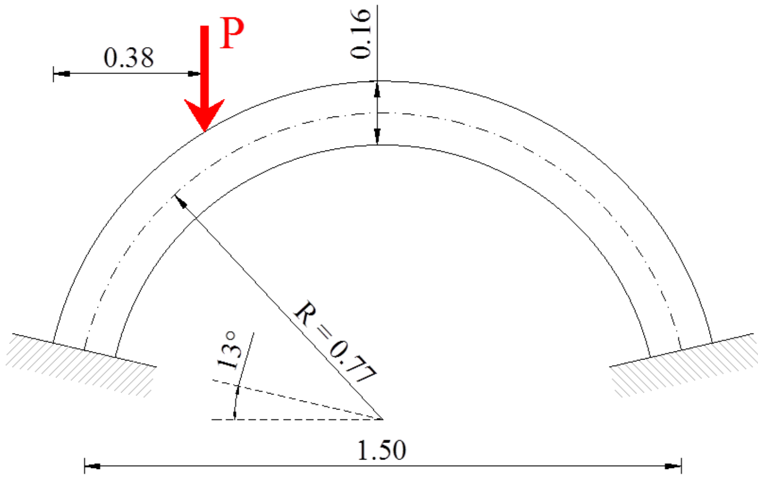

Figure 1: Geometry of the arch (length in meters).

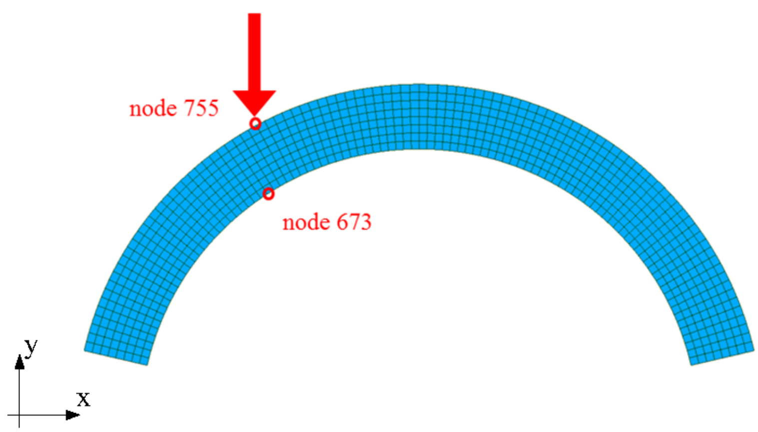

Figure 2: Mesh of the arch created by NOSA-ITACA code.

The numerical analyses conducted with NOSA-ITACA, MARC and DIANA have manifold goals. Firstly, they are aimed at analysing the static behavior of the arch modeled by adopting three different constitutive equations. Secondly they allow comparing the natural frequencies of the arch in the linear elastic case with those in the presence of the damage induced by the increasing vertical load. Several parametric numerical experiments have been carried out, as the tensile strength σ_t of the material varies, revealing that, in the presence of cracks, the values of the frequencies calculated by the three codes are comparable.

A preliminary modal analysis (step 1, Section 2) was performed by assuming the arch made of a linear elastic material with Young's modulus $E = 3 \cdot 10^9$ Pa, Poisson's ratio $\nu = 0.2$ and mass density $\rho = 1930\,\mathrm{kg/m^3}$. The first four corresponding natural frequencies $f_{\mathrm{i,E}}$ (i = 1...4) (calculated by the three codes) are

$$f_{1,\mathrm{E}} = 92.33\ \mathrm{Hz};\ f_{2,\mathrm{E}} = 163.64\ \mathrm{Hz};\ f_{3,\mathrm{E}} = 266.95\ \mathrm{Hz};\ f_{4,\mathrm{E}} = 297.95\ \mathrm{Hz}.$$

Then, by following the procedure outlined in Section 2, step 2, damage was induced in the arch by applying the self-weight along with an incremental vertical load. At each increment the frequencies $f_{\mathrm{i,j}}$ (the i-th frequency calculated by j-th code: N (NOSA-ITACA), M (MARC) and D(DIANA)) and the corresponding mode shapes were calculated.

In order to perform nonlinear static analysis in DIANA and MARC, the parameters $G_{\mathrm{f}}^{\mathrm{I}}$ and E_s (see Section 2) have to be assigned, in addition to the tensile strength σ_t, set to vary from 0 Pa to $5 \cdot 10^4$ Pa. The Mode-I fracture

energy with $G_{\rm f}^{\rm I} = 25$ Nm/m^2 was assumed in DIANA, while E_s was calculated, for each analysis performed in MARC, by imposing the equivalence between the areas below the softening curves of both codes.
The value of the vertical load applied to the arch was increased through eight increments from 0 kN to 4 kN. Each analysis was repeated by decreasing the value of σ_t from $5 \cdot 10^4$ Pa to $5 \cdot 10^3$ Pa. For values of σ_t lower than $5 \cdot 10^3$ Pa, only NOSA-ITACA and DIANA reach the convergence for any value of the vertical load.

It is pointed out that in terms of displacement, stress and cracking fields, the results provided by the three codes show very good agreement for each value of the vertical load up to a tensile stress of $5 \cdot 10^3$ Pa. Figures 3, 4, 5, 6 and 7 display for the three codes the plots relevant to the norm of displacements, the components of the Cauchy stress tensor and the maximum eigenvalue of the fracture strain, calculated for $\sigma_t = 5 \cdot 10^3$ Pa and P $= 4$ kN. Despite the different constitutive equations adopted, NOSA-ITACA and DIANA provide the same results, whereas the values obtained in MARC exhibit an increment of about $5 - 10\%$ with respect to the afore-mentioned codes.

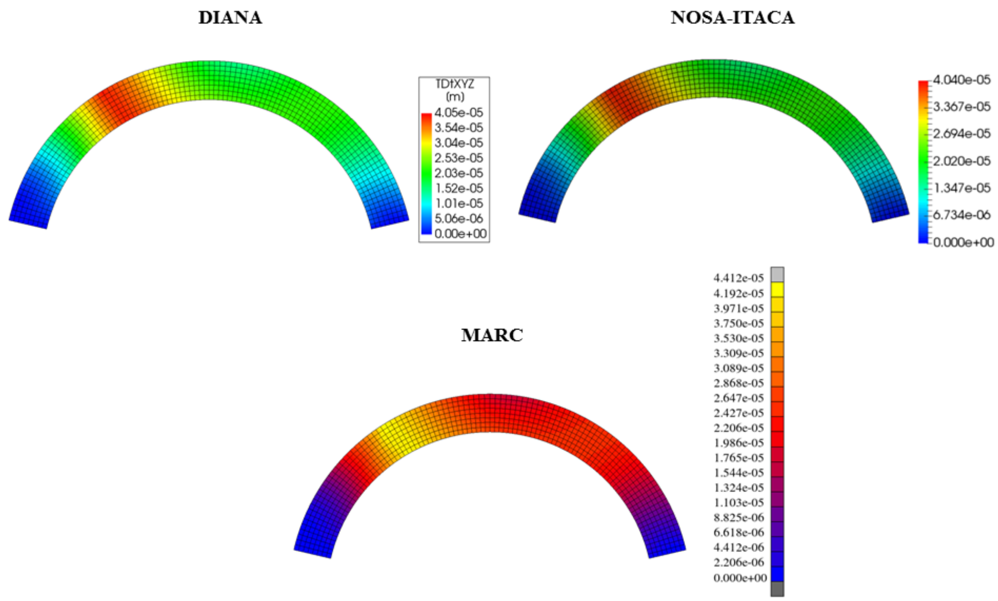

Figure 3: Norm of displacement [m] (P = 4 kN, $\sigma_t = 5 \cdot 10^3$ Pa).

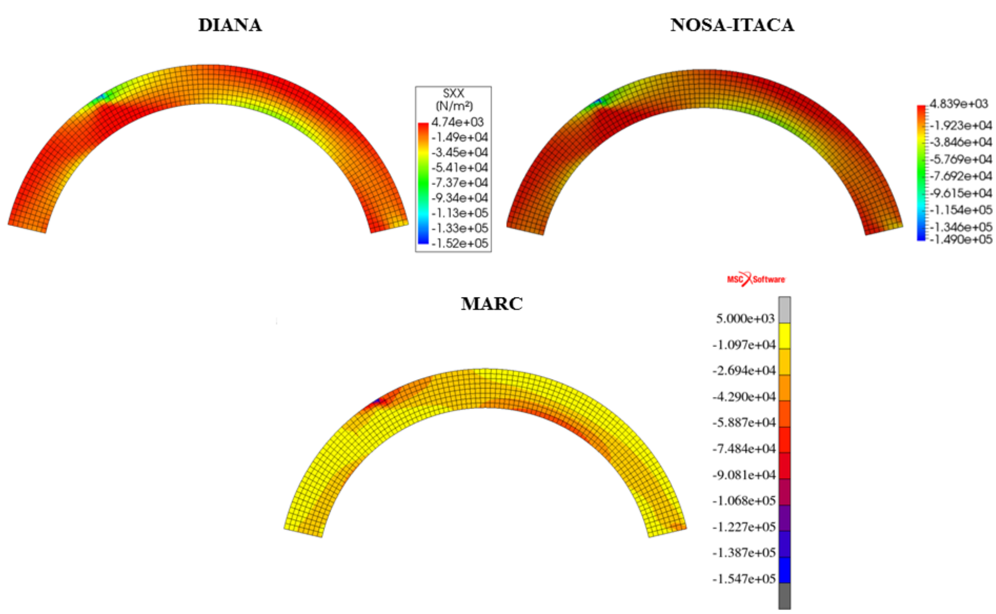

Figure 4: Cauchy stress component σ_x [Pa] (P = 4 kN, $\sigma_t = 5 \cdot 10^3$ Pa).

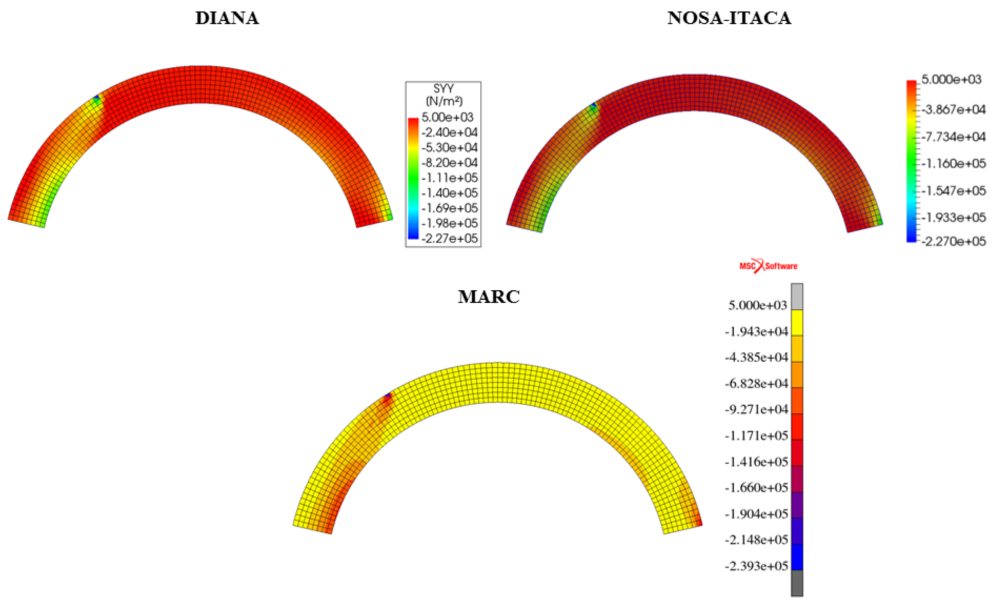

Figure 5: Cauchy stress component σ_y [Pa] (P = 4 kN, $\sigma_t = 5 \cdot 10^3$ Pa).

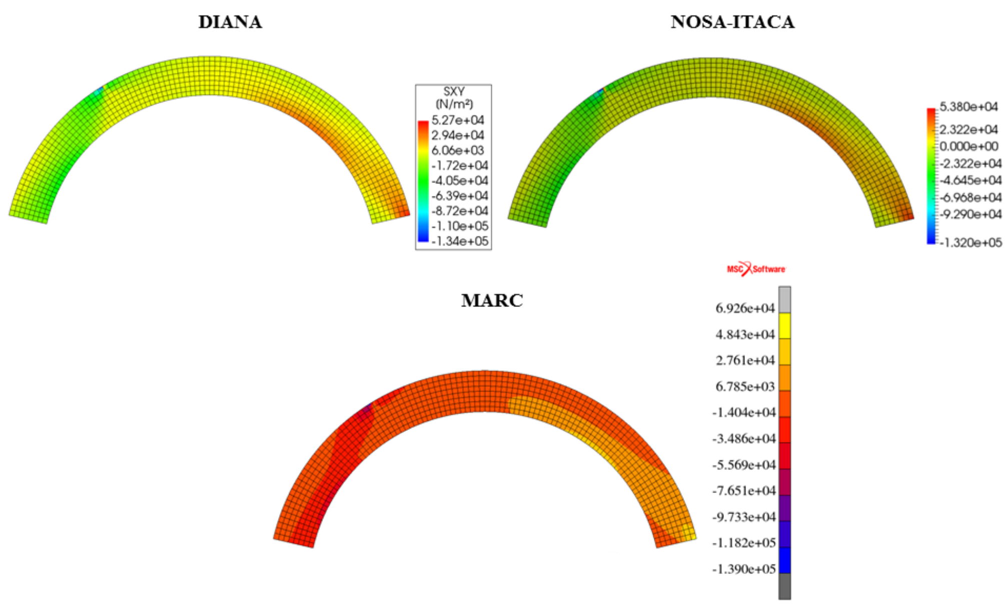

Figure 6: Cauchy stress component τ_{xy} [Pa] (P = 4 kN, $\sigma_t = 5 \cdot 10^3$ Pa).

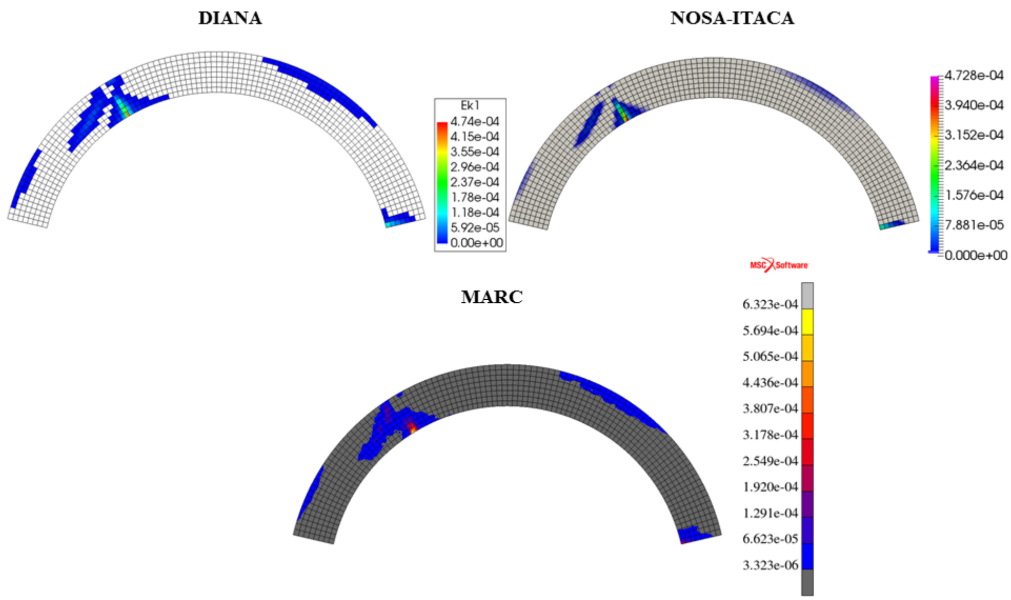

Figure 7: Maximum eigenvalue of the fracture strain tensor (P = 4 kN, $\sigma_t = 5 \cdot 10^3$ Pa).

Figures 8, 9, 10, 11 show the variation of the first four frequencies $f_{\rm i,j}$ of the arch, calculated in the three codes via linear perturbation analysis, versus decreasing values of tensile strength σ_t for P = 3 kN (continuous line) and P = 4 kN (dashed line). The corresponding mode shapes for the linear elastic case are also shown. Tables 1, 2, and 3, 4 report, for the same load conditions P, the values of σ_t used in the different analyses along with the corresponding relative frequency errors $\delta_{\rm i,j}$ defined by

$$\delta_{\rm i,j} = \frac{(f_{\rm i,E} - f_{\rm i,j})}{f_{\rm i,E}}, \quad \text{for i} = 1...4 \ \text{ and j} = \text{N, M, D} \tag{5}$$

where $f_{\rm i,E}$ is the i-th frequency calculated by standard modal analysis and $f_{\rm i,j}$ the i-th frequency calculated by j-th code via linear perturbation analysis, (N stands for NOSA-ITACA, M for MARC and D for DIANA).

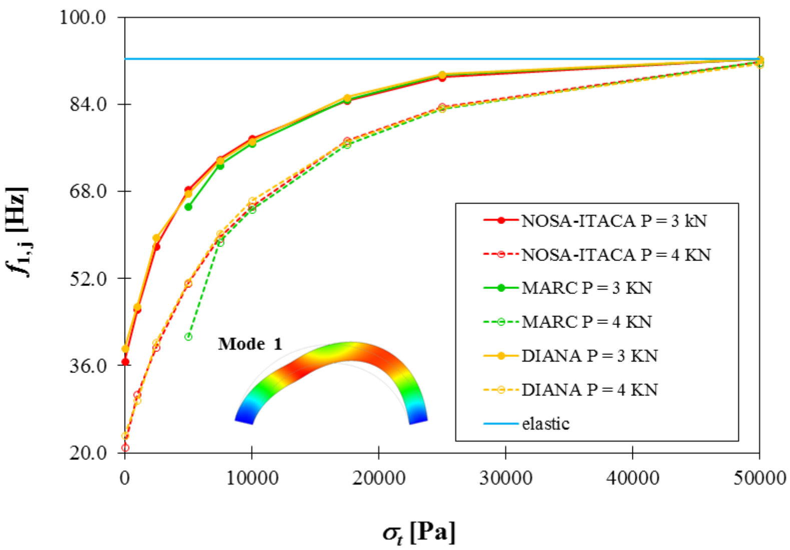

Figure 8: First frequency $f_{1,\text{j}}$ versus tensile strength σ_t for P = 3 kN (continuous line) and P = 4 kN (dashed line).

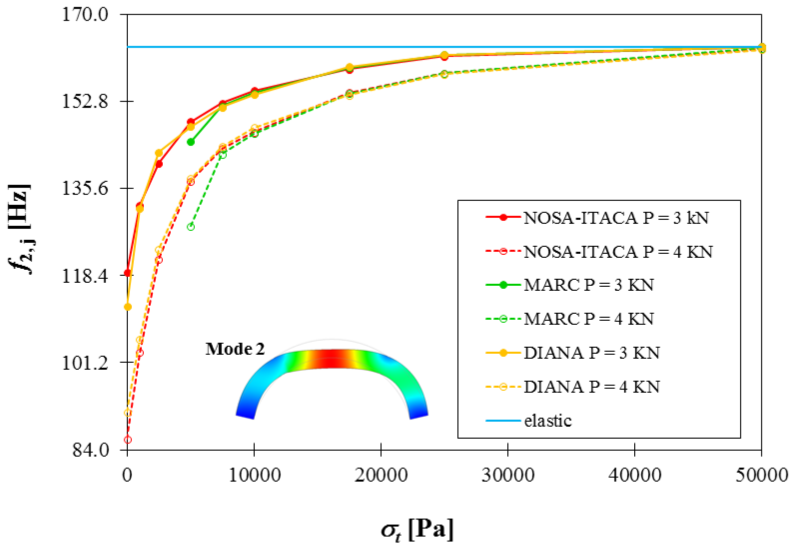

Figure 9: Second frequency $f_{2,\mathrm{j}}$ versus tensile strength σ_t for P = 3 kN (continuous line) and P = 4 kN (dashed line).

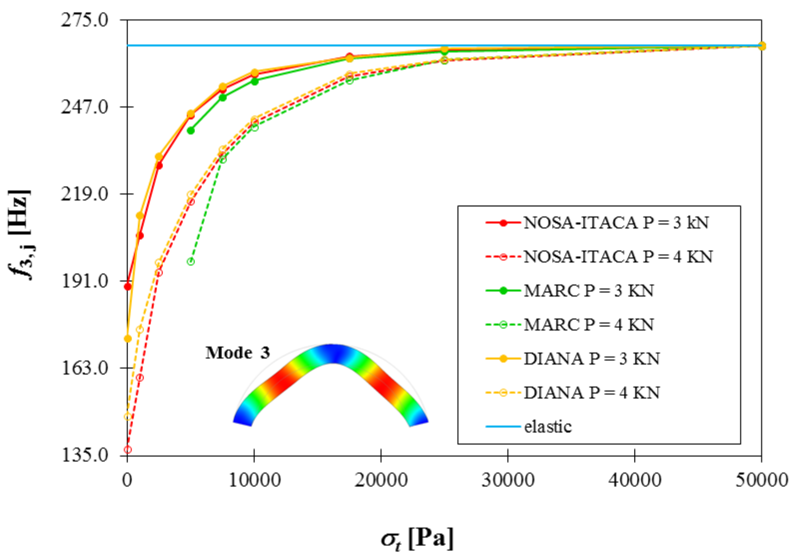

Figure 10: Third frequency $f_{3,\mathrm{j}}$ versus tensile strength σ_t for P = 3 kN (continuous line) and P = 4 kN (dashed line).

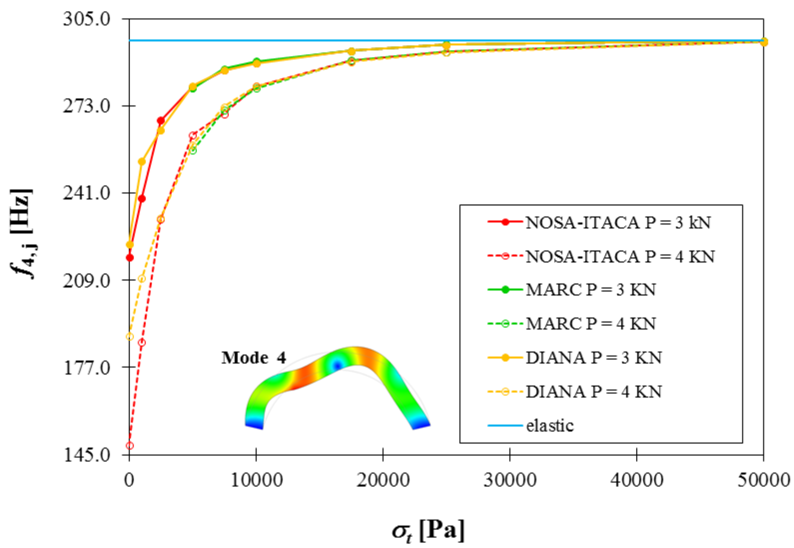

Figure 11: Fourth $f_{4,\mathrm{j}}$ versus tensile strength σ_t for P = 3 kN (continuous line) and P = 4 kN (dashed line).

σ_t[Pa]	$\delta_{1,\mathrm{N}}$[%]	$\delta_{1,\mathrm{M}}$[%]	$\delta_{1,\mathrm{D}}$[%]	$\delta_{2,\mathrm{N}}$[%]	$\delta_{2,\mathrm{M}}$[%]	$\delta_{2,\mathrm{D}}$[%]
0	60.20	–	57.61	27.28	–	31.28
1000	49.80	–	49.13	19.09	–	19.47
2500	37.21	–	35.52	14.03	–	12.74
5000	25.93	29.35	26.68	9.06	11.45	9.63
7500	19.81	21.07	20.19	6.79	7.15	7.26
10000	15.80	16.77	16.26	5.32	5.60	5.75
17500	8.20	8.06	7.57	2.67	2.51	2.38
25000	3.56	3.06	2.89	1.14	0.95	0.95
50000	0.00	0.00	0.00	0.00	0.00	0.00

Table 1: $\delta_{\mathrm{i,j}}$, i = 1,2 ; j = N, M, D ; P = 3 kN.

σ_t[Pa]	$\delta_{3,\mathrm{N}}$[%]	$\delta_{3,\mathrm{M}}$[%]	$\delta_{3,\mathrm{D}}$[%]	$\delta_{4,\mathrm{N}}$[%]	$\delta_{4,\mathrm{M}}$[%]	$\delta_{4,\mathrm{D}}$[%]
0	28.95	–	35.24	26.71	–	25.08
1000	22.86	–	20.45	19.43	–	14.92
2500	14.42	–	13.31	9.81	–	10.99
5000	8.36	10.21	8.17	5.66	5.88	5.56
7500	5.29	6.24	4.92	3.63	3.47	3.65
10000	3.52	4.30	3.19	2.69	2.54	2.77
17500	1.35	1.57	1.47	1.21	1.19	1.21
25000	0.60	0.70	0.39	0.50	0.41	0.45
50000	0.00	0.00	0.00	0.00	0.00	0.00

Table 2: $\delta_{\mathrm{i,j}}$, i = 3,4 ; j = N, M, D ; P = 3 kN.

σ_t[Pa]	$\delta_{1,\mathrm{N}}$[%]	$\delta_{1,\mathrm{M}}$[%]	$\delta_{1,\mathrm{D}}$[%]	$\delta_{2,\mathrm{N}}$[%]	$\delta_{2,\mathrm{M}}$[%]	$\delta_{2,\mathrm{D}}$[%]
0	77.20	–	74.92	47.38	–	44.10
1000	66.79	–	67.90	36.94	–	35.28
2500	57.29	–	56.32	25.63	–	24.42
5000	44.50	55.15	44.38	16.19	21.67	15.91
7500	35.57	36.42	34.72	12.32	12.95	12.03
10000	29.27	29.94	28.12	10.32	10.50	9.76
17500	16.15	17.01	16.45	5.53	5.62	5.81
25000	9.42	9.80	9.66	3.19	3.20	3.28
50000	0.56	0.51	0.95	0.19	0.17	0.34

Table 3: $\delta_{\mathrm{i,j}}$, i = 1,2 ; j = N, M, D ; P = 4 kN.

σ_t[Pa]	$\delta_{3,\mathrm{N}}[\%]$	$\delta_{3,\mathrm{M}}[\%]$	$\delta_{3,\mathrm{D}}[\%]$	$\delta_{4,\mathrm{N}}[\%]$	$\delta_{4,\mathrm{M}}[\%]$	$\delta_{4,\mathrm{D}}[\%]$
0	48.70	–	44.65	50.06	–	36.55
1000	40.01	–	34.17	37.21	–	29.39
2500	27.26	–	26.15	22.03	–	21.90
5000	18.79	26.05	17.98	11.59	13.52	12.88
7500	13.17	13.71	12.54	9.02	8.58	8.16
10000	9.26	9.82	8.84	5.62	5.83	5.60
17500	3.72	4.24	3.45	2.46	2.40	2.55
25000	1.79	1.76	1.70	1.35	1.34	1.43
50000	0.08	0.08	0.04	0.08	0.07	0.13

Table 4: $\delta_{\mathrm{i,j}}$, i = 3,4 ; j = N, M, D ; P = 4 kN.

As expected, the figures highlight that the frequencies of the arch decrease as the vertical load increases and the tensile strength decreases. As outlined in Tables 1, 2, 3 and 4, regardless of the value of the vertical load, the fundamental frequency falls faster than the other frequencies; approximately 27% against 9%, when P = 3 kN and $\sigma_t = 5 \cdot 10^3$ Pa, and 50% against 20%, when P = 4 kN and $\sigma_t = 5 \cdot 10^3$ Pa. This is due to the chosen vertical load position, which induces a deformation in the arch similar to the first mode shape (Figure 12, 13).

Figure 12 shows the mode shapes corresponding to the first four frequencies of the arch for $\sigma_t = 5 \cdot 10^3$ Pa and P = 3 kN. Figure 13 shows the same four mode shapes but for $\sigma_t = 5 \cdot 10^3$ Pa and P = 4 kN. The figures report the degree of consistency, expressed in terms of MAC, viz. Modal Assurance Criterion [31] , calculated between the i-th mode shape of the damaged arch and the corresponding mode shape calculated via standard modal analysis. It is noticed that frequencies are much more sensitive than mode shapes to damage; for example when $\sigma_t = 5 \cdot 10^3$ Pa and P $= 3$ kN, the first frequency shows a relative variation of about 25% while the MAC value is equal to 0.99, whereas when $\sigma_t = 5 \cdot 10^3$ Pa and P $= 4$ kN, the first frequency has a relative downshift of about 50% (which indeed corresponds to a severe damage condition), but the MAC still continues to be rather high, showing values not lower than 0.90.

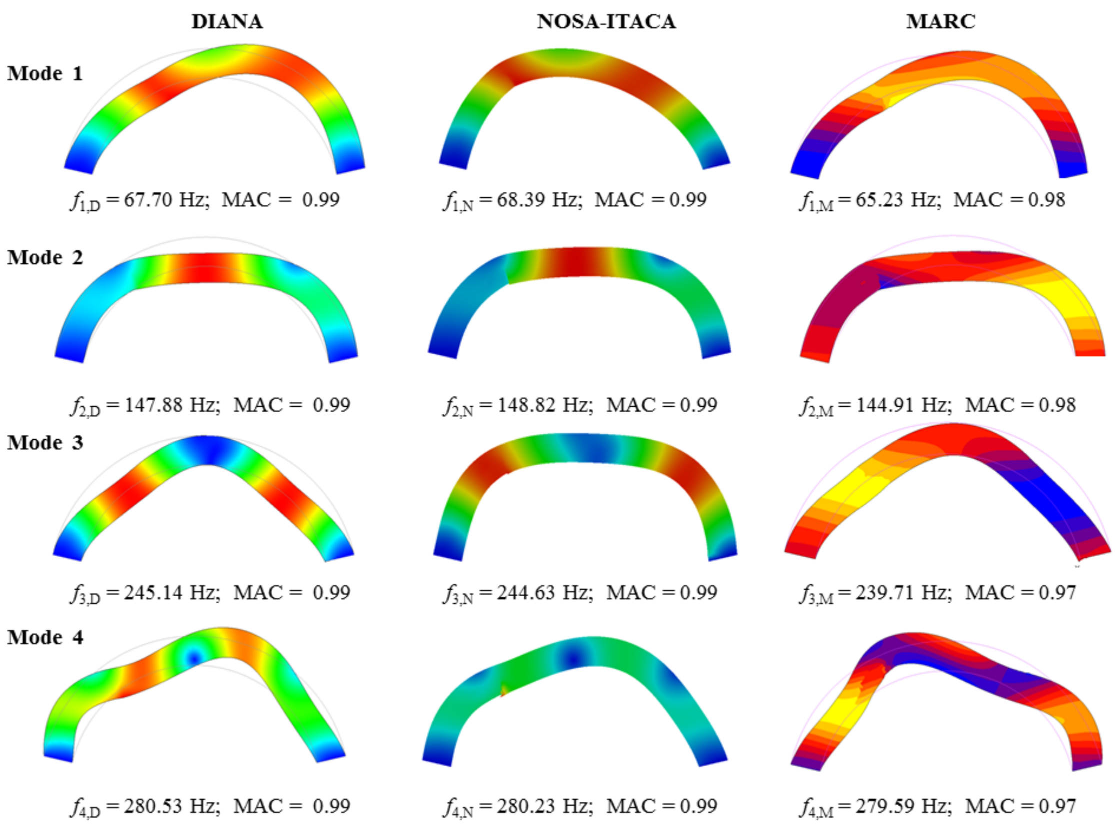

Figure 12: First four mode shapes of the damaged arch (P $= 3$ kN, $\sigma_t = 5 \cdot 10^3$ Pa).

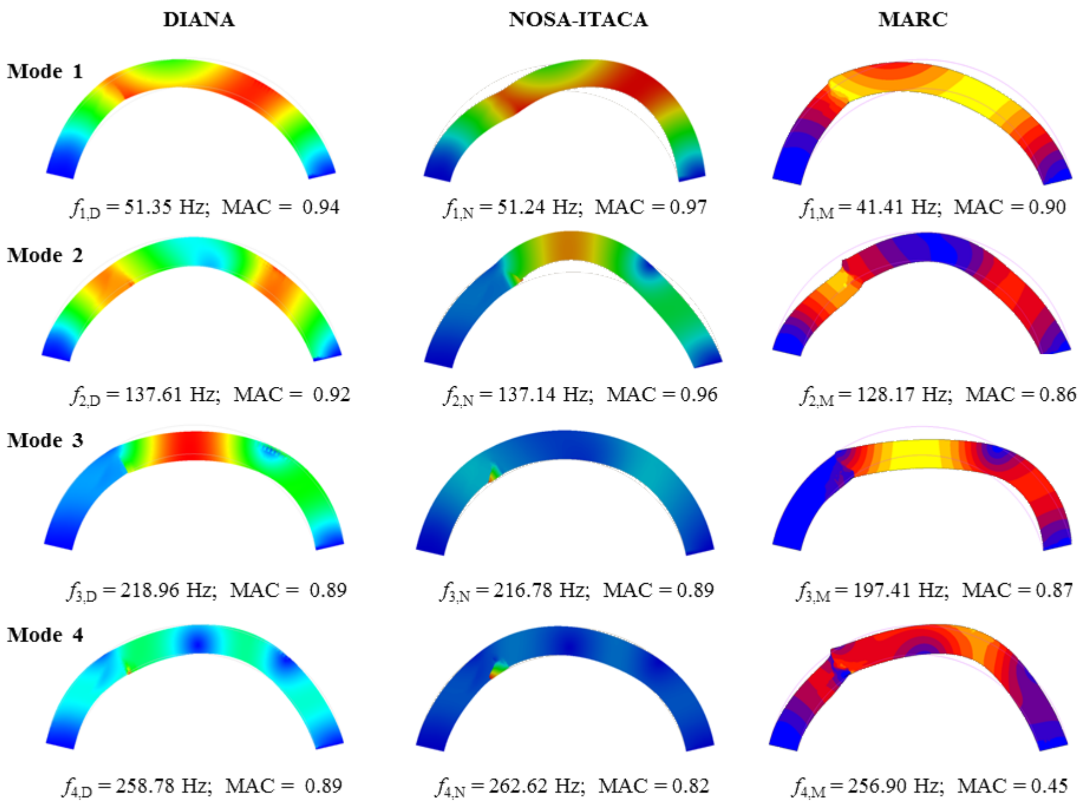

Figure 13: First four mode shapes of the damaged arch (P = 4 kN, $\sigma_t = 5 \cdot 10^3$ Pa).

In order to validate the frequencies values calculated by the three FE codes, the load-displacement curves corresponding to $\sigma_t = 5 \cdot 10^3$ Pa were plotted (Figure 14) for nodes 755 and 673, positioned respectively at the application point of vertical load and the corresponding point at the intrados of the arch (Figure 2).

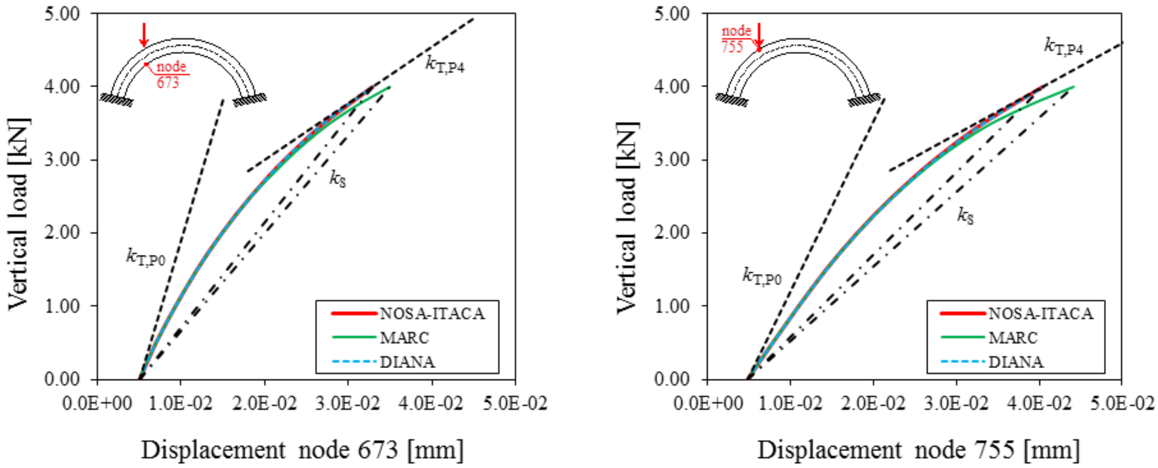

Figure 14: Vertical load versus displacement magnitude of node 673 (on the left) and node 755 (on the right), $\sigma_t = 5 \cdot 10^3$ Pa.

For each curve, its fourth-degree interpolating polynomial is determined and then the slopes $k_{\mathrm{T,P0}}$ and $k_{\mathrm{T,P4}}$ of the tangents at the origin and at P = 4 kN, (dashed lines in Figure 14) are calculated. The slope k_{S} of the secant passing for those points (dashed-dot lines in Figure 14) is also calculated. Since the loss of frequency is expected to be related to the square root of the loss of stiffness (mass being equal), the following quantities were calculated as for the first frequency, i.e. the one suffering a major decrease due to damage

$$\tilde{f}_{1,\mathrm{T}} = f_{1,\mathrm{E}} \cdot \sqrt{\frac{k_{\mathrm{T,P4}}}{k_{\mathrm{T,P0}}}}, \tag{6}$$

$$\tilde{f}_{1,\mathrm{S}} = f_{1,\mathrm{E}} \cdot \sqrt{\frac{k_{\mathrm{S}}}{k_{\mathrm{T,P0}}}}, \tag{7}$$

The results obtained are summarized in Tables 5 and 6 for all the three codes. It is worth noting that the first frequency $\tilde{f}_{1,\mathrm{T}}$ calculated by using the tangent stiffness is a good approximation of the frequency $f_{1,\mathrm{j}}$ computed via linear perturbation analysis, whereas the choice of the secant stiffness matrix would lead to an overestimation of the frequency of the damaged structure.

Code	P [kN]	k_{T} [kN/m]	k_{S} [kN/m]	$\tilde{f}_{1,\mathrm{T}}$ [Hz]	$\tilde{f}_{1,\mathrm{S}}$ [Hz]	$f_{1,\mathrm{j}}$ [Hz]
N	0	254.48	143.52	50.87	69.34	51.24
	4	77.26				
M	0	260.23	133.68	41.76	66.18	41.41
	4	53.23				
D	0	254.48	143.55	50.88	69.34	51.35
	4	77.28				

Table 5: Comparison of the first frequency of the arch using the tangent stiffness k_{T} and the secant stiffness k_{S} evaluated in node 673 with the numerical frequency obtained via linear perturbation analysis.

Code	P [kN]	k_{T} [kN/m]	k_{S} [kN/m]	$\tilde{f}_{1,\mathrm{T}}$ [Hz]	$\tilde{f}_{1,\mathrm{S}}$ [Hz]	$f_{1,\mathrm{j}}$ [Hz]
N	0	180.68	112.31	54.16	72.79	51.24
	4	62.16				
M	0	173.20	133.68	46.54	70.75	41.41
	4	53.23				
D	0	180.68	114.69	54.78	73.56	51.35
	4	63.61				

Table 6: Comparison of the first frequency of the arch using the tangent stiffness k_{T} and the secant stiffness k_{S} evaluated in node 755 with the numerical frequency obtained via linear perturbation analysis.

4. Application to a real case study: the Mogadouro clock tower

4.1. Description of the case study

The Mogadouro clock tower (Figure 15) is a historic masonry structure located inside the castle perimeter of the homonymous town in the Northeast of Portugal and likely built after 1559 to serve the neighbouring church as a bell tower. The fabric features a rectangular cross section of 4.7 x4.7 m^2, with masonry walls of about 1 m thickness, and a height of 20.4 m. The central part of the walls is built of rubble stones with thick mortar joints, whereas the corners are made of large granite units with dry joints. Eight masonry columns support the roof body, forming two rectangular openings of about 0.9 x2.0 m^2 per façade.

Figure 15: Clock tower and castle of Mogadouro.

Due to the lack of maintenance, the tower did appear in very poor conditions. Beyond material degradation and biological growth, out-of-plane displacements and cracks could be clearly observed. The most damaged parts were the East and West façades, where two deep passing cracks were about to separate the box cross section of the tower into two U halves (Figures 16, 17). As the structural safety was jeopardized, rehabilitation works aimed at reinstating the sound condition of the structure were carried out in 2005. The intervention included: lime grout injections for sealing and walls consolidation, substitution of deteriorated material, and installation of pre-stressed tie-rods to restrain cracks from possible reopening.

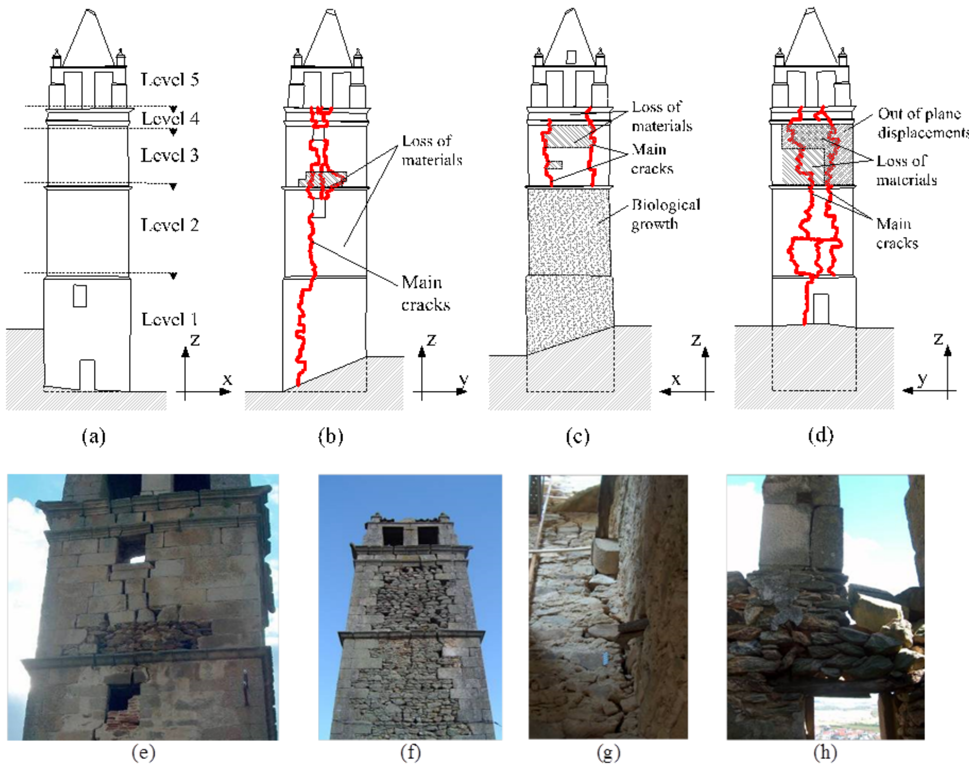

Figure 16: Damage in the tower: (a) South, (b) East, (c) North and (d) West façades; cracks on the (e) East and (f) West fronts; (g) inner crack in the West façade; and (h) example of material loss [44], [45].

4.2. Dynamic identification of the tower before and after rehabilitation

To evaluate the structural response pre- and post-rehabilitation, two campaigns of Ambient Vibrations Tests (AVTs) were carried out making use of ambient excitation sources, such as wind and traffic [44], [45]. The response of the tower was measured in 54 selected points distributed along three levels, according to the layout displayed in Figure 17. The dynamic equipment consisted of 4 uniaxial piezoelectric accelerometers with a bandwidth ranging from 0.15 to 1000 Hz (5%), a dynamic range of $\pm$0.5g, a sensitivity of

10 V/g, 8μg of resolution and 0.21 kg of weight, connected by coaxial cables to a front-end data acquisition system with a 24-bit ADC, provided with anti-aliasing filters. The front-end was connected to a laptop by an Ethernet cable. The accelerometers were bolted to aluminium plates, which were in turn glued to the stones through an epoxy layer. As the acquisition system was composed only by 4 channels, 27 test setups were necessary to record the accelerations in all selected measurement points. A preliminary FE dynamic analysis assisted in the selection of the acquisition parameters. Thus, to ensure an acquisition time window 2000 times larger than the estimated fundamental period of the structure, the output signals were recorded with a sampling frequency of 256 Hz for a duration of about 11 minutes. Same test planning and measurement points were adopted before and after the reinstatement works.

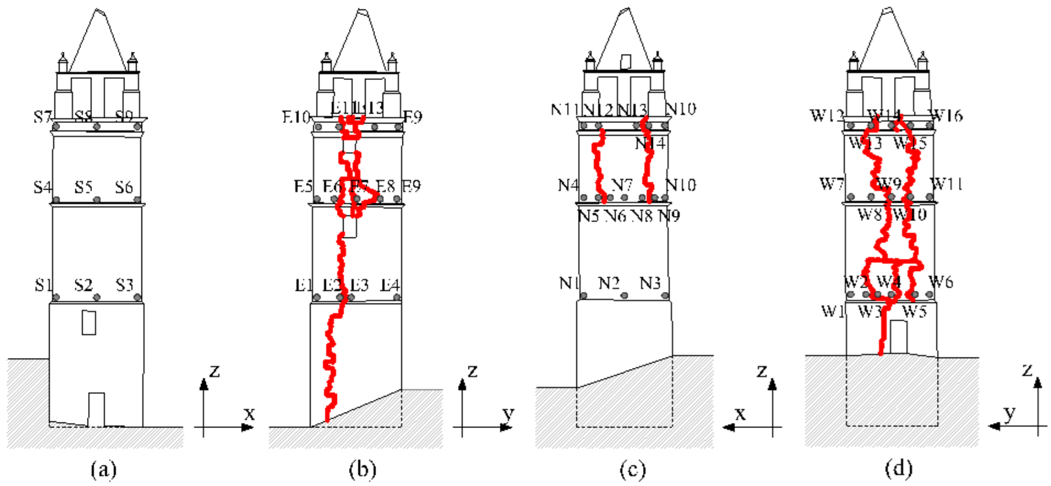

Figure 17: Sensor layout for AVTs: (a) South, (b) East, (c) North and (d) West façades [44], [45].

For each structural condition (before and after rehabilitation), the modal parameters were estimated by comparing the results from two established and complementary OMA techniques: the Enhanced Frequency Domain Decomposition (EFDD) method and the Stochastic Subspace Identification (SSI) method, both implemented in ARTeMIS software [3]. In total, seven modes of vibration were identified in the frequency ranges 2-9 Hz and 2-17 Hz for the damaged and undamaged conditions, respectively. Tables 7 and 8 summarize the obtained results in terms of natural frequencies $f_{\mathrm{i,exp}}$, damping ratios $\xi_{\mathrm{i,exp}}$, Coefficient of Variation CV and percentage differences Δ before and after rehabilitation. Mode shapes and MAC values are illustrated in

Figure 18. For the sake of brevity, only the modal features identified by the SSI are shown.

Mode	Before		After		$\Delta_f[\%]$
	$f_{\mathrm{i,exp}}$[Hz]	$\mathrm{CV}_f[\%]$	$f_{\mathrm{i,exp}}$[Hz]	$\mathrm{CV}_f[\%]$	
1	2.15	1.85	2.56	0.21	+19.28
2	2.58	1.05	2.76	0.30	+6.70
3	4.98	0.69	7.15	0.27	+43.67
4	5.74	1.56	8.86	0.47	+54.37
5	6.76	1.13	9.21	0.21	+36.13
6	7.69	2.94	15.21	2.24	+97.87
7	8.98	1.21	16.91	1.40	+88.27
Avg	–	1.49	–	0.73	+49.47

Table 7: Dynamic response of Mogadouro tower before and after rehabilitation in terms of frequencies [44], [45].

Mode	Before		After		$\Delta_\xi[\%]$
	$\xi_{\mathrm{i,exp}}[\%]$	$\mathrm{CV}_\xi[\%]$	$\xi_{\mathrm{i,exp}}[\%]$	$\mathrm{CV}_\xi[\%]$	
1	2.68	219.51	1.25	0.13	-53.26
2	1.71	94.02	1.35	0.17	-21.00
3	2.05	65.33	1.20	0.14	-41.32
4	2.40	24.27	1.31	0.13	-45.72
5	2.14	31.74	1.16	0.12	-45.65
6	2.33	55.98	2.54	0.24	+9.11
7	2.30	46.39	1.49	0.23	-35.07
Avg	2.23	76.75	1.47	0.17	-40.34

Table 8: Dynamic response of Mogadouro tower before and after rehabilitation in terms of damping [44], [45].

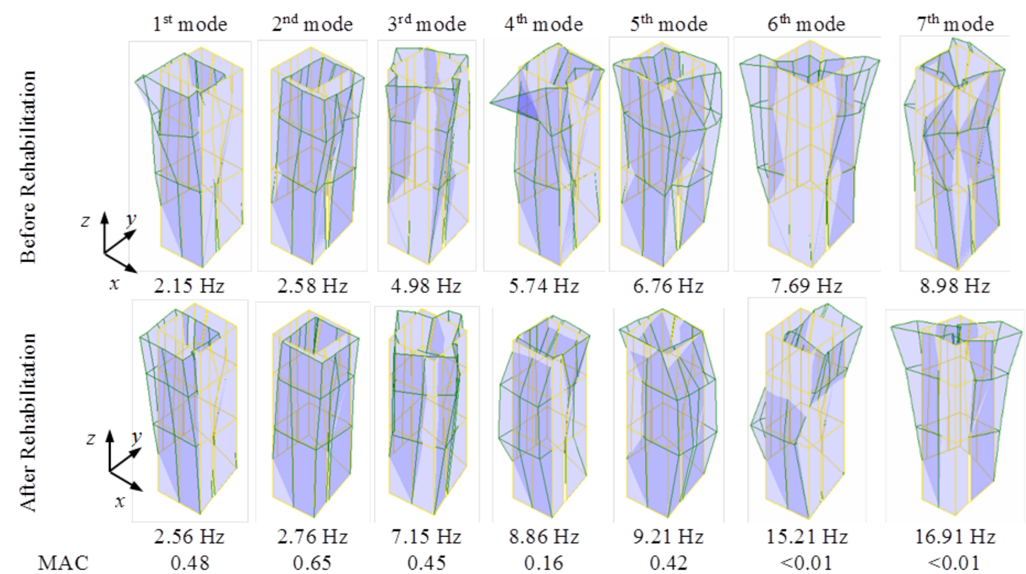

Figure 18: Experimental mode shapes and MAC values before and after rehabilitation works [44].

The comparison between the global parameters estimated before and after the consolidation works revealed a significant increase of frequency values, reading an average upshift of 50%, and a damping decrease of around 40%. Such results consistently reflected the actual structural conditions of the tower, i.e. a lower-stiffness system with ongoing non-linear phenomena effects before rehabilitation and a higher-stiffness system with reduced non-linear phenomena effects after rehabilitation. In what concerns the experimental mode shapes, similar configurations were observed pre- and post-intervention for the first five modes of vibration, identifying four dominant bending modes in the two main planes of the tower (modes $1, 2, 4$ and 5) and one torsional mode (mode 3), whereas higher-frequency mode shapes (modes 6 and 7) switched order after the works. Although comparable in configuration, the presence of local damage mechanisms before the structural intervention did likely induce local protuberances in the experimental mode shapes of the damaged tower, especially in the upper part of the structure and in the areas close to the cracks. Hence the poor degree of correlation characterizing the mode shape vectors before and after (MAC < 0.65). On the contrary, the structure featured a monolithic behaviour after the rehabilitation works.

4.3. Modal analysis with linear perturbation

In this subsection the linear perturbation analysis is applied to the Mogadouro clock tower. The analysis is performed by using only NOSA-ITACA code for two reasons: (1) in DIANA, the Rankine plasticity model describing the tensile regime of the material is implemented only for plane stress, plane strain and axisymmetric elements, but not for brick elements, which are the ones employed in modeling the tower; (2) the MARC code turned out to be unable to reach the convergence for $\sigma_t = 0$ Pa, a value that is crucial for a realistic modeling of eastern and western façades, where two passing cracks were present before rehabilitation.

In [44] and [45] a FE model updating (based on standard modal analysis) is performed to tune the Young's modulus of different parts of the structure, in order to minimize the differences between numerical and experimental modal parameters (frequencies and mode shapes) of the tower after rehabilitation; subsequently, the Young's moduli obtained are reduced with the aim of fitting the experimental frequencies and mode shapes of the tower before rehabilitation. Here, a different approach is followed, based on model updating aimed at matching both fracture distribution and frequencies of the tower. With the purpose of reproducing numerically the actual crack pattern of the tower before rehabilitation and matching its experimental frequencies as well, **the scheme described in Section 2 (nonlinear static analysis – linear perturbation – modal analysis) has been applied in an iterative way.** In particular, once the solution to the equilibrium problem of the structure subjected to its own weight is calculated along with the corresponding fracture distribution, linear perturbation analysis and modal analysis are conducted to estimate frequencies and mode shapes of the tower in the presence of cracks. The materials Young's moduli and tensile strengths are tuned and their optimal values calculated **in such a way as to match the crack distribution and minimize the discrepancy between experimental and numerical frequencies**. The same procedure was then repeated to tune the tensile strength of the repaired walls, keeping the Young's moduli fixed and trying to match the experimental natural frequencies and mode shapes of the tower after rehabilitation.

The FE mesh of the tower, shown in Figure 19, consists of 18024 isoparametric 8−node brick elements, 352 thick shell elements, used to discretize the roof, and 23467 nodes; the model includes also two meters of foundation [44], [45] with the same thickness as the façades. The tower is assumed to be clamped at the base and constituted by the materials whose (optimal) mechanical properties, calculated via model updating, are indicated in Table 9. The foundation is modeled by a linear elastic material, which is indeed an acceptable assumption considering the high material compaction at the base of the tower and the soil confinement. Regarding pillars and roof, the use of a linear elastic material is suggested by the observation that these elements do not affect the overall structural behavior of the tower. Indeed, the low elastic modulus adopted for the roof does allow the tower cross section to freely deform within its own plane.

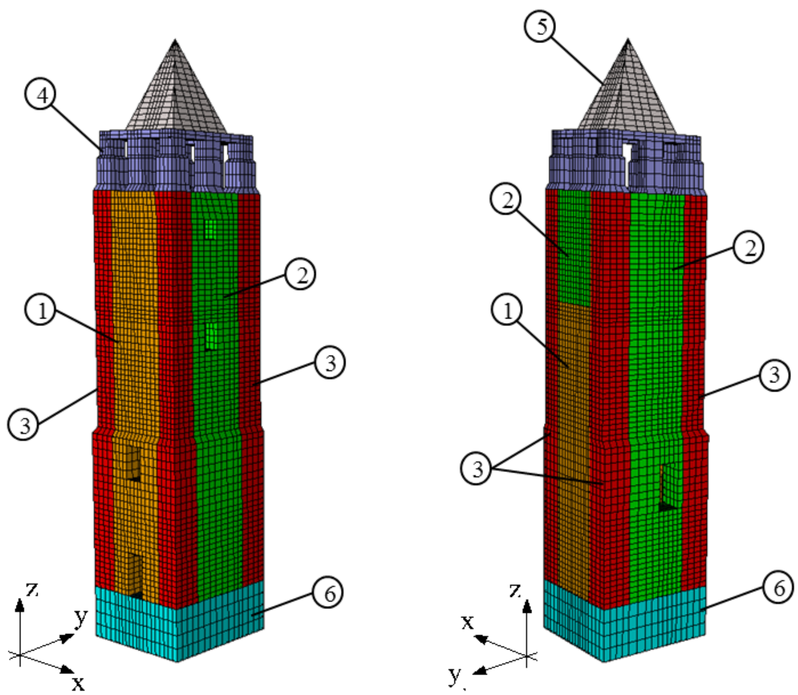

Figure 19: Mogadouro tower, mesh and distribution of material properties (before rehabilitation).

Mat. n°	Tower's portion	$\varrho[kg/m^3]$	$E[GPa]$	$\sigma_t[kPa]$
1 (orange)	façades South and North (bottom)	2200	2.500	15.0
2 (green)	façades East, West and North (top)	2200	2.500	0.0
3 (red)	corners	2400	3.500	15.0
4 (indigo)	pillars	2200	1.210	–
5 (grey)	roof	2000	0.195	–
6 (cyan)	foundation	2200	3.500	–

Table 9: Optimal values of the material mechanical properties before rehabilitation.

Numerical solution to the equilibrium problem for the optimal values of the Young's moduli and tensile strengths in Table 9 yields the results reported in Figures 20, 21 and 22 that show, for each façade, the actual (on the left) and numerical (on the right) crack patterns before rehabilitation. The South wall is not reported because it shows no cracks (neither in the numerical model nor in the reality). A very good agreement can be observed between real and numerical fracture strains.

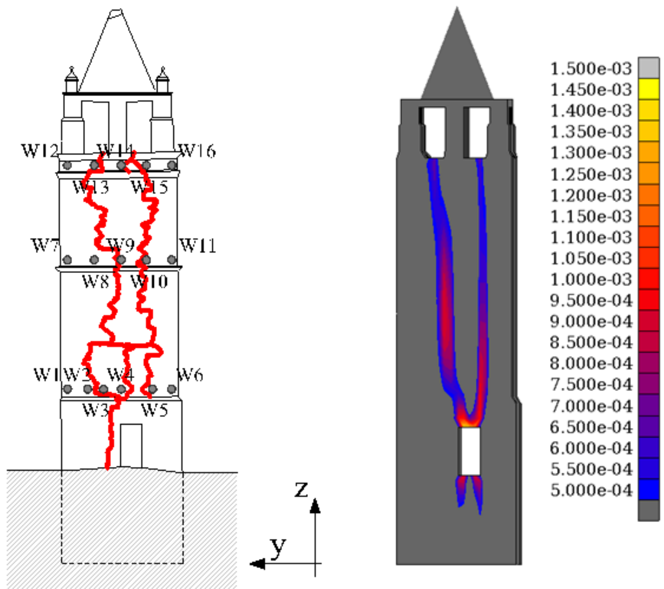

Figure 20: Mogadouro tower West façade, surveyed (on the left) and numerical (on the right) cracking pattern.

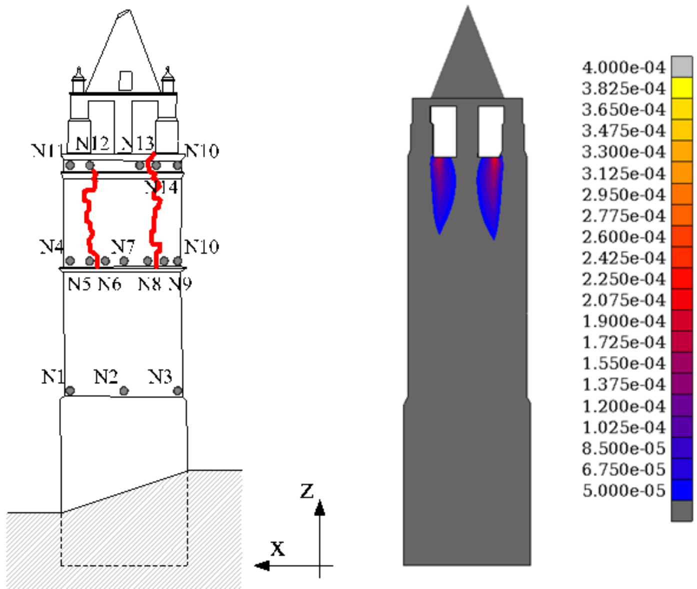

Figure 21: Mogadouro tower North façade, surveyed (on the left) and numerical (on the right) cracking pattern.

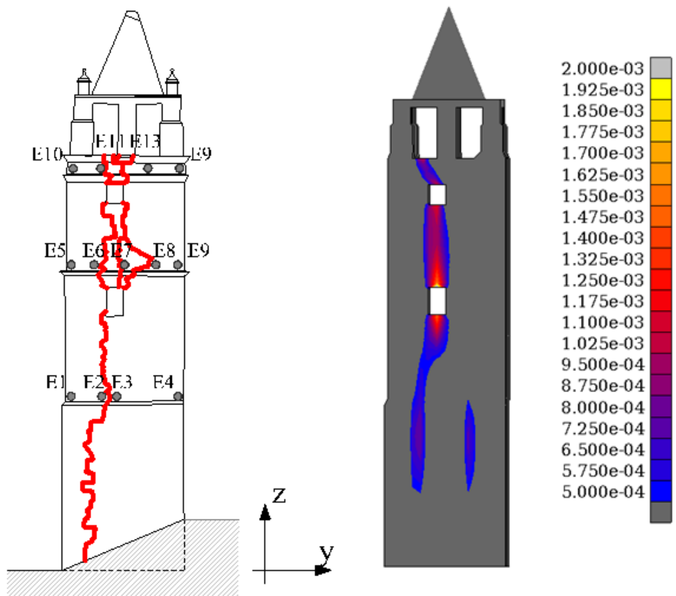

Figure 22: Mogadouro tower East façade, surveyed (on the left) and numerical (on the right) cracking pattern.

Table 10 summarizes the results of the modal analysis before rehabilitation in terms of experimental ($f_{\mathrm{i,exp}}$) and numerical ($f_{\mathrm{i,N}}$) frequencies, relative frequency error, and MAC values between experimental and numerical mode shapes (evaluated considering just the nodes monitored during the experimental campaigns [44], [45]). The four frequencies and the first two mode shapes are very well approximated, while the correlation of the third and fourth numerical mode shapes with their experimental counterparts is quite low (particularly for the fourth mode). **The poor match between the third experimental and numerical mode shapes before rehabilitation is inherent to the adopted modeling strategy and likely due to the fact that, as far as the numerical solution is concerned, passing cracks in the East and West façades do not allow the tower's section to undergo torsional deformations. On the contrary, in the real case, such a deformation is made possible by interlocking effect and friction between the units. It is also possible that other (non-visible damage) can affect this mode.**

Mode	$f_{\mathrm{i,exp}}$ [Hz]	$f_{\mathrm{i,N}}$ [Hz]	Δ_f[%]	MAC
1	2.15	2.15	0.00	0.94
2	2.58	2.60	-0.78	0.96
3	4.98	4.92	1.20	0.32
4	5.74	5.88	-2.44	0.01

Table 10: Comparison between experimental ($f_{\mathrm{i,exp}}$) and numerical frequencies ($f_{\mathrm{i,N}}$); relative frequency error $\Delta_f = (f_{\mathrm{i,exp}} - f_{\mathrm{i,N}})/f_{\mathrm{i,exp}}$ and MAC values before rehabilitation.

Figure 23 shows the first four experimental and numerical (calculated by NOSA-ITACA) mode shapes of the Mogadouro tower before rehabilitation.

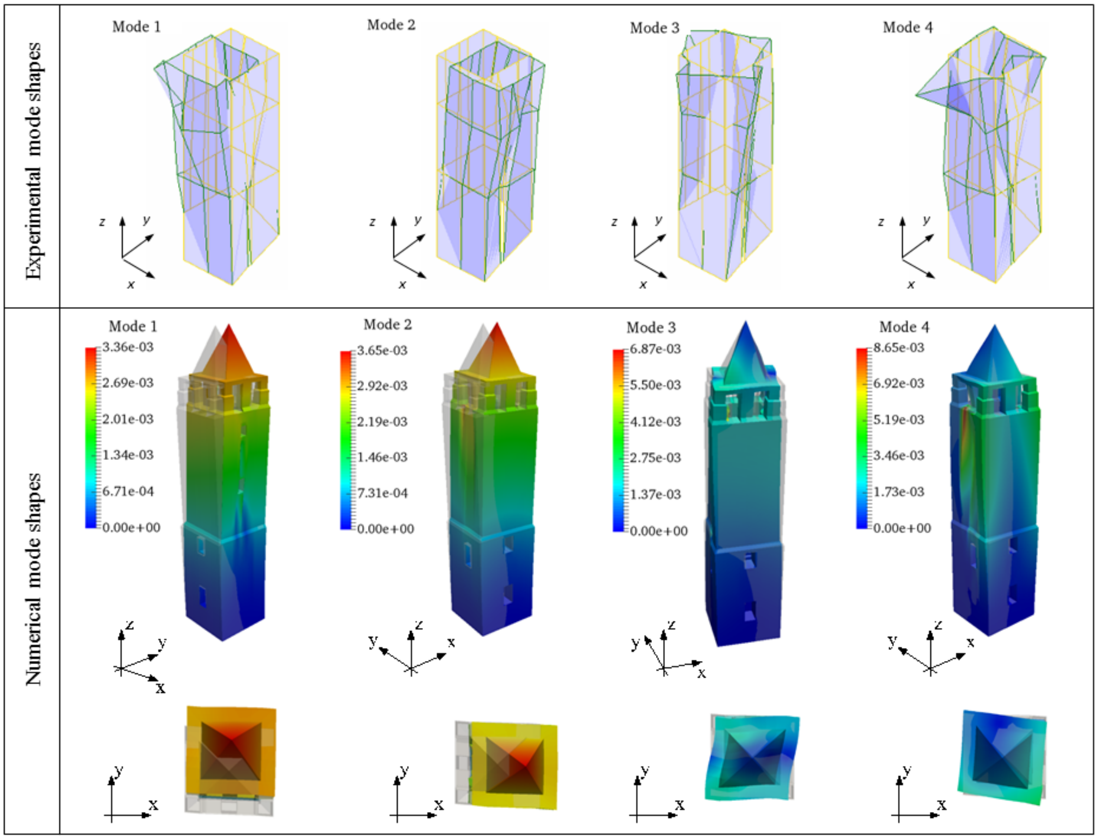

Figure 23: **First four mode shapes of the Mogadouro tower before rehabilitation.**

Subsequently, the same FE model is adopted to perform the analysis of the tower after rehabilitation, considering a tensile strength $\sigma_t = 10\,\text{kPa}$ for the restored walls (material 2 in Figure 19), while the other mechanical properties are kept fixed.

The results are summarized in table 11; **Figure 24 shows the first four experimental and numerical mode shapes after rehabilitation**. All frequencies increase with respect to the unreinforced case, consistently with the experimental results. In this case, a good approximation is achieved for all four mode shapes, and a very great accuracy is obtained in the assessment of the first two frequencies.

Mode	$f_{\mathrm{i,exp}}$ [Hz]	$f_{\mathrm{i,N}}$ [Hz]	Δ_f[%]	MAC
1	2.56	2.59	-1.17	0.98
2	2.76	2.75	0.36	0.98
3	7.15	8.39	-17.34	0.97
4	8.86	9.32	-5.19	0.74

Table 11: Comparison between experimental ($f_{\mathrm{i,exp}}$) and numerical frequencies ($f_{\mathrm{i,N}}$); relative frequency error $\Delta_f = (f_{\mathrm{i,exp}} - f_{\mathrm{i,N}})/f_{\mathrm{i,exp}}$ and MAC values after rehabilitation.

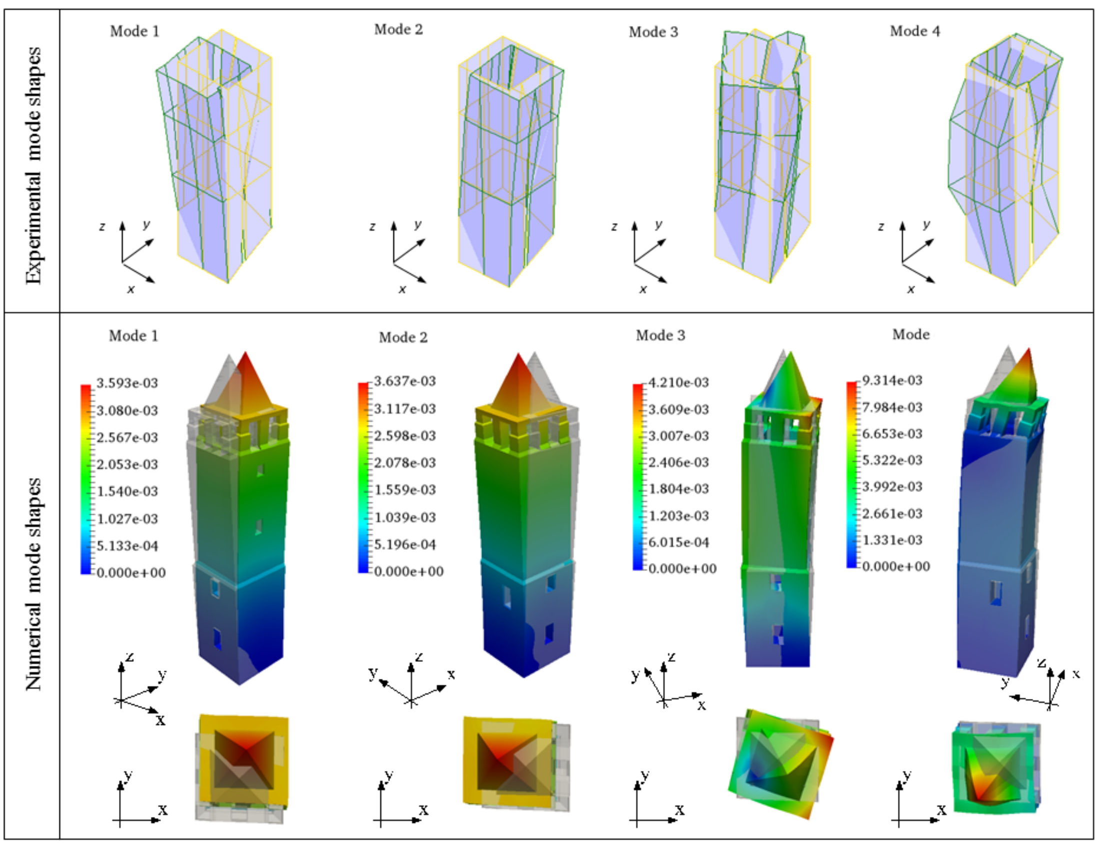

Figure 24: **First four mode shapes of the Mogadouro tower after rehabilitation.**

Table 12 recapitulates experimental and numerical results in terms of natural frequencies, before and after rehabilitation of the tower, pointing out that the linear perturbation analysis allows to catch the dynamic behavior of the structure in damaged conditions with reasonable accuracy. The table shows also that the numerical increase of the natural frequencies, due to restoration of the tower and obtained in the numerical model through an increase of tensile strength of the damaged walls, is in agreement with the experimental results, apart from the third frequency, which is overestimated by the code.

Mode	Before		After		Δ_f[%]	
	$f_{\mathrm{i,exp}}$ [Hz]	$f_{\mathrm{i,N}}$ [Hz]	$f_{\mathrm{i,exp}}$ [Hz]	$f_{\mathrm{i,N}}$ [Hz]	exp	num
1	2.15	2.15	2.56	2.59	+19.28	+20.46
2	2.58	2.60	2.76	2.75	+6.70	+5.77
3	4.98	4.92	7.15	8.39	+43.67	+70.52
4	5.74	5.88	8.86	9.32	+54.37	+58.50

Table 12: Summary of the experimental and numerical results before and after rehabilitation.

For the sake of comparison, the optimal values of the Young's modulus E_{S} calculated via a model updating based on standard modal analysis [44], [45] are reported in table 13 together with the corresponding values E_{NL} obtained by a model updating based on linear perturbation analysis. As expected, in the standard modal analysis the lowest values of the Young's modulus are obtained in the cracked façades.

	Before		After	
	$E_S[GPa]$	$E_{LP}[GPa]$	$E_S[GPa]$	$E_{LP}[GPa]$
South façade	0.687	2.500	1.974	2.500
North façade	2.210	2.500	2.210	2.500
West façade	0.302	2.500	1.075	2.500
East façade	0.276	2.500	0.804	2.500
Corners	3.870	3.500	3.875	3.500

Table 13: Comparison between the optimal values of the Young's modulus E_S (standard modal analysis) and E_{LP} (linear perturbation and modal analysis).

Tables 14 and 15 show the frequencies and MAC values calculated via standard modal analysis and linear perturbation analysis, before and after rehabilitation; for the sake of completeness the experimental frequencies are reported as well.

Mode	$f_{i,exp}$ [Hz]	Linear Perturbation			Standard		
		f_i [Hz]	Δ_f[%]	MAC	f_i [Hz]	Δ_f[%]	MAC
1	2.15	2.15	0.00	0.94	2.07	3.72	0.97
2	2.58	2.60	-0.78	0.96	2.40	6.98	0.97
3	4.98	4.92	1.20	0.32	5.14	-3.21	0.96
4	5.74	5.88	-2.44	0.01	5.88	-2.44	0.73

Table 14: Comparison between the frequencies calculated via standard modal analysis and linear perturbation before rehabilitation.

Mode	$f_{\mathrm{i,exp}}$ [Hz]	Linear Perturbation			Standard		
		f_{i} [Hz]	Δ_f[%]	MAC	f_{i} [Hz]	Δ_f[%]	MAC
1	2.56	2.59	-1.17	0.98	2.54	0.78	0.99
2	2.76	2.75	0.36	0.98	2.68	2.90	0.99
3	7.15	8.39	-17.34	0.97	7.33	-2.52	1.00
4	8.86	9.32	-5.19	0.74	8.62	2.71	0.98

Table 15: Comparison between the frequencies calculated via standard modal analysis and linear perturbation after rehabilitation.

5. Conclusions

The present paper investigated the dependence of the dynamic properties of masonry structures on the nonlinear behavior of the constituent materials. As the mechanical response of masonry constructions is remarkably different in tension and in compression, and cracks may arise due permanent and accidental loads, standard modal analysis may result unrealistic. In this context, a linear perturbation approach must be used to adequately estimate the dynamic properties of masonry constructions in the presence of cracked regions. After a brief description of the constitutive equations and numerical procedures implemented in different FE codes (NOSA-ITACA, DIANA and MARC), the proposed approach, which couples linear perturbation and modal analysis, is described. The numerical procedure is then applied to a masonry arch with the aim of comparing and cross-validating the results obtained from the afore-mentioned FE codes in terms of natural frequencies and mode shapes for decreasing values of tensile strength. It is demonstrated that, despite the different constitutive equations the three codes rely on, the dependence of the dynamic properties of the masonry arch on the applied loads and induced crack distribution is consistent among the three of them, showing comparable frequency downshifts and MAC values over the different damage scenarios. Finally, with the purpose of validating the same approach on a real case-study structure, the procedure is applied to a historic masonry tower affected by a serious crack pattern. After solving the nonlinear equilibrium problem of the structure subjected to its own weight and reproducing the actual fracture distribution, a modal analysis about the equilibrium solution is carried out to estimate frequencies and mode shapes of the tower in the presence of cracks as well as after the rehabilitation works. A FE model updating is used to tune the optimal values for both Young's modulus and tensile strength in the different parts of the tower, according to the observed structural conditions before and after the intervention. **The comparison between numerical and experimental results showed that the combination of linear perturbation and modal analysis enables to estimate with reasonable accuracy the first two frequencies and mode shapes of the masonry tower in both damaged and reinforced conditions. The method proposed seems to be promising and further applications are necessary to confirm the reliability of the adopted approach for the solution of the dynamic problem in case of structures built with masonry materials.**

Acknowledgements. This research has been partially supported by the Region of Tuscany (PAR-FAS 2007 – 2013) and MIUR, the Italian Ministry of Education, Universities and Research (FAR) within the Call FAR-FAS 2014 (MOSCARDO Project: ICT technologies for structural monitoring of age-old constructions based on wireless sensor networks and drones, 2016 – 2018) and by the Research Program Short–Term Mobility, funded by CNR, "Models, methods and tools for the structural analysis of ancient masonry constructions", 2018. These supports are gratefully acknowledged.

[1] Alemdar Bayraktar, Ahmet Can Altunisik,Baris Sevim and Temel Türker, Seismic response of a historical masonry minaret using a finite element model updated with operational modal testing. *Journal of Vibration and Control*, 17(1): 129-149, 2011.

[2] Altunisik A. C., Okur F. Y. , Fuat Genç A. , Günaydin, M., and Adanur, S., Automated model updating of historical masonry structures based on ambient vibration measurements. *Journal of Performance of Constructed Facilities*, 32(1): 04017126, 2018.

[3] Artemis Manual, Structural Vibration Solutions A/S, 2006.

[4] Azzara R.M., De Roeck G., Girardi M., Padovani C., Pellegrini D., Reynders E., The influence of environmental parameters on the dynamic behaviour of the San Frediano bell tower in Lucca. *Engineering Structures*, 156: 175-187, 2018.

[5] Azzara R.M., De Falco A., Girardi M.,Pellegrini D., Ambient vibration recording on the Maddalena bridge in Borgo a Mozzano (Italy): Data analysis. *Annals of Geophysics*, 60(4): S0441, 2018.

[6] Bartoli G., Betti M., Vignoli A., A numerical study on seismic risk assessment of historic masonry towers: a case study in San Gimignano *A. Bull Earthquake Eng* 14: 1475, 2016.

[7] Bassoli E., Vincenzi L., D'Altri A.M, De Miranda S., Forghieri M., Castellazzi G., Ambient vibration-based finite element model updat-

ing of an earthquake-damaged masonry tower. *Structural Control and Health Monitoring*, 25(5): e2150, 2018.

[8] Binante V, Girardi M, Padovani C, Pasquinelli G, Pellegrini D, Porcelli M., Robol L. *NOSA-ITACA 1.1 documentation* 2017. www.nosaitaca.it/software/.

[9] Buyukozturk O., Nonlinear analysis of reinforced concrete structures. *Comput Struct*, 7: 149-156, 1977.

[10] Cabboi A., Gentile C. , Saisi A., From continuous vibration monitoring to FEM-based damage assessment: Application on a stone-masonry tower. *Construction and Building Materials* 156: 252-265, 2017.

[11] Camacho G.T., and Ortiz M., Computational modelling of impact damage in brittle materials. *Int J Solids Struct* 33: 2899-2938, 1996.

[12] Conde B., Ramos L.F. , Oliveira D.V., Riveiro B., Solla M., Structural assessment of masonry arch bridges by combination of non-destructive testing techniques and three-dimensional numerical modelling: Application to Vilanova bridge. *Engineering Structures* 148: 621-638, 2017.

[13] Debabrata Das, A new tangent stiffness-based formulation to study the free vibration behavior of a transversely loaded Timoshenko beam

with geometric nonlinearity. *Journal of Vibration and Control*; **24(9)**: 1716-1727, 2018.

[14] Del Piero G., Constitutive equation and compatibility of the external loads for linearly-elastic masonry-like materials. *Meccanica* 24: 150-62, 1989.

[15] *DIANA-10.2 Finite Element Analysis, User's Manual-Release 10.2.* TNO, Netherlands, 2017.

[16] Dolatshahi K.M., Aref A.J., Yekrangnia M., Bidirectional behavior of unreinforced masonry walls. *Earthq. Eng. Struct. Dyn.* 43: 2377-2397, 2014.

[17] Dolatshahi K.M., Aref A.J., Whittaker A.S., Interaction curves for in-plane and out-of-plane behaviors of unreinforced masonry walls. *J. Earthq. Eng.* 19: 60-84, 2015.

[18] Formisano A., Florio G., Landolfo R., Krstevska L., Tashkov Lj., Experimental and numerical investigation on a monumental masonry buiding damaged by the Abruzzo earthquake *8th International Conference on Structural Analysis of Historical Constructions SAHC 2012*, 2012.

[19] Feenstra P.H., Borst R., A plasticity model and algorithm for mode-I cracking in concrete. *Int. J. Numer. Methods Engrg.* 38: 2509-2529, 1995.

[20] Feenstra P.H., Borst R., Crack band theory for fracture of concrete. *Materials and Structures*, RILEM, 93(16): 155-177, 1983.

[21] Gentile C., Guidobaldi M. and Saisi A., One-year dynamic monitoring of a historic tower: damage detection under changing environment. *Meccanica*, 51(11):2873–2889, 2016.

[22] Girardi M., Padovani C., Pellegrini D., The NOSA-ITACA code for the safety assessment of ancient constructions: A case study in Livorno. *Advances in Engineering Software* 89: 64-76, 2015.

[23] Girardi M., Padovani C., Pellegrini D., Modal analysis of masonry structures. *Mathematics and Mechanics of Solids*, First Published February 13, doi.org/10.1177/1081286517751837, 2018.

[24] Harak SS, Sharma SC, Harsha SP. Modal analysis of prestressed draft pad of freight wagons using finite element method. *J. Mod. Transport* 2015; **23(1)**:43–49.

[25] Lagomarsino S., Penna A., Galasco A., Cattari S., TREMURI program: An equivalent frame model for the nonlinear seismic analysis of masonry buildings. *Enginnering Structures* 56: 1787-1799, 2013.

[26] Lourenço P.B. , Oliveira D.V. , Milani G., Computational advances in masonry structures: from mesoscale modelling to engineering application. *Developments and Applications in Computational Structures Technology Saxe-Coburg Publications*, Chapter 1, pp. 1-23, 2010.

[27] Lourenço P.B. Computations on historic masonry structures. *Prog. Struct. Engng Mater.* 4: 301-319, 2002

[28] Lourenço P.B., Mendes N., Oliveira D.V. ,L.F. Ramos Possibilities and comparison of structural component models for the seismic assessment of modern unreinforced masonry buildings. *Computers and Structures* 89, 2079-2091, 2011

[29] Lourenço P.B., Mendes N., Oliveira D.V. ,L.F. Ramos Analysis of masonry structures without box behavior. *International Journal of Architectural Heritage* 5:4-5, 369-382, 2011

[30] Lucchesi M., Padovani C., Pasquinelli G., Zani N. *Masonry constructions: mechanical models and numerical applications* 2008; Lecture Notes in Applied and Computational Mechanics. Springer–Verlag.

[31] Maia N.M.M. and Silva J.M.M. *Theoretical and experimental modal analysis*. Research Studies Press LTD., Baldock, Hertfordshire, England, 1997.

[32] *Marc 2014 Volume A: theory and user information.* Marc & Mentat (2014) - Marc & Mentat Docs.

[33] Masciotta M.G., Ramos L.F., Lourenço P.B., The importance of structural monitoring as a diagnosis and control tool in the restoration process of heritage structures: A case study in Portugal. *Journal of Cultral Heritage* 27: 36-47, 2017.

[34] Masciotta M.G., Ramos L.F., Lourenço P.B., Vasta M. Damage identification and seismic vulnerability assessment of a historic masonry chimney. *Annals of Geophysics* 60(4),2017. doi: 10.4401/ag-7126 2017.

[35] Mistler M., Butenweg C., Meskouris K., Modelling methods of historic masonry buildings under seismic excitation. *J Seismol* 10: 497-510, 2006.

[36] Noble D, Nogal M, O'Connor AJ, Pakrashi V. The effect of post-tensioning force magnitude and eccentricity on the natural bending frequency of cracked post-tensioned concrete beams, *Journal of Physics. Conference Series 628*, 2015. IOPscience.

[37] Oliveira D.V., Lourenço P.B., Implementation and validation of a constitutive model for the cyclic behaviour of interface elements. *Comput Struct* 82: 1451-61, 2004.

[38] Padovani C., Silhavy M., On the derivative of the stress-strain relation in a no-tension material. *Mathematics and Mechanics of Solids* 22: 1606-1618, 2017.

[39] Pantò B., Cannizzaro F., Caliò I, Lourenço P.B., Numerical and experimental validation of a 3D macro-model for the in-plane and out-of-plane behavior of unreinforced masonry walls. *International Journal of Architectural Heritage* 11.7: 946-964, 2017.

[40] Peeters B. and De Roeck G. One–year monitoring of the Z24–Bridge: enviromental effects versus gamage events *Earthquake engineering and structural dynamics,* 30: 149–171, 2001.

[41] Pineda P. Collapse and upgrading mechanisms associated to the structural materials of a deteriorated masonry tower. Nonlinear assessment under different damage and loading levels. *Engineering Failure Analysis* 2016; **63**:72–93, Elsevier.

[42] Quagliarini E., Maracchini G., Clementi F. Uses and limits of the equivalent frame model on existing unreinforced masonry buildings for assessing their seismic risk: A review. *Journal of Building Engineering* 10: 166-182, 2017.

[43] Ramos LF, De Roeck G, Lourenço PB, Campos–Costa A. Damage identification on arched masonry structures using ambient and random impact vibrations. *Engineering Structures* 2010; **32**: 146–162, Elsevier.

[44] L.F. Ramos , L. Marques , P.B. Lourenço , G.De Roeck , A. Campos-Costa and J.Roque. Monitoring historical masonry structures with operational modal analysis: two case studies. *Mech. Syst. Signal Process.* 24: 1291-1305, 2010.

[45] L.F. Ramos Damage identification on masonry structures based on vibration signatures *Ph.D Thesis, University of*

Minho, Portugal. **Available from www.hms.civil.uminho.pt, 2007**

[46] Ramos L.F., Núñez García A.C., Fernandes F.M. , Lourenço P.B. . Evaluation of structural intervention in the Quartel das Esquadras, Almeida (Portugal). *Mech. Syst. Signal Process.* 24: 1291-1305, 2010.

[47] Rots J.G., Blaauwendraad J., Crack models for concrete, discrete or smeared? Fixed, multi-directional or rotating?. *HERON* 34.1, ISSN: 0046-7316, 1989.

[48] Sacco E., A non linear homogenization procedure for periodic masonry. *Eur J Mech A/Solids* 28: 209-22, 2009.

[49] Sarhosis, Vasilis, Katalin Bagi, José V. Lemos, and Gabriele Milani, *Computational Modeling of masonry structures using the discrete element method*, IGI Global, 2016. 1-505. Web. 16 May. 2018. doi: 10.4018/978-1-5225-0231-9.

[50] Silva L.C., Lourenço P.B., Milani, G., Nonlinear discrete homogenized model for out-of-plane loaded masonry walls. *Journal of Structural Engineering (United States)* 143.9: 1451-61, 2017.

[51] Taliercio A., Binda L., The Basilica of San Vitale in Ravenna: investigation on the current structural faults and their mid-term evolution. *J Cultural Heritage* 8: 99-118, 2007.

[52] Torres W., Almazán J.L., Sandoval C., Boroschek R., Operational modal analysis and FE model updating of the Metropolitan Cathedral of Santiago, Chile, *Engineering Structures* 143: 169-188, 2017.

[53] Treyssède F., Finite element modeling of temperature load effects on the vibration of local modes in multi-cable structures, *Journal of Sound and Vibration* 413: 191–204, 2018.